Molecular imaging of gene expression in living subjects by spliceosome-mediated RNA trans-splicing

S. Bhaumik*, Z. Walls*, M. Puttaraju†, L. G. Mitchell†, and S. S. Gambhir*‡

*Department of Radiology and Bio-X Program, Stanford University, James H. Clark Center E150, 318 Campus Drive, Stanford, CA 94305-5427; and †Intronn Inc., 910 Clopper Road, South Building, Suite 210, Gaithersburg, MD 20878

Communicated by Michael E. Phelps, University of California School of Medicine, Los Angeles, CA, April 19, 2004 (received for review February 2, 2004)

Spliceosome-mediated RNA trans-splicing (SMaRT) provides an effective means to reprogram mRNAs and the proteins they encode. SMaRT technology has a broad range of applications, including RNA repair and molecular imaging, each governed by the nature of the sequences delivered by the pre-trans-splicing molecule. Here, we show the ability of SMaRT to optically image the expression of an exogenous gene at the level of pre-mRNA splicing in cells and living animals. Because of the modular design of pre-trans-splicing molecules, there is great potential to employ SMaRT to image the expression of any arbitrary gene of interest in living subjects. In this report, we describe a model system that demonstrates the feasibility of imaging gene expression by trans-splicing in small animals. This represents a previously undescribed approach to molecular imaging of mRNA levels in living subjects.

mRNA repair | gene correction | reporter

In the postgenomic era, a great impetus has been generated toward designing therapeutic and diagnostic agents that are able to capitalize on the wealth of genetic information now available. Although proteins are the ultimate effectors of genetic programming, there are several preceding steps in the cascade of gene expression where interventions for therapy or diagnosis are possible. Because of the complex tertiary folding and singular structure of each individual protein, it is unfeasible (at present) to design molecules specific for an arbitrary protein based on sequence alone. However, given that the principles behind targeting arbitrary nucleic acid sequences have been well established (1) and our profound knowledge of the human genomic sequence, it is practicable to design molecules that interact with specific genes at the nucleotide level. By exploiting the Watson–Crick base-pairing nature of nucleic acids, researchers have been able to design sequence-specific molecules for purposes ranging from *in vivo* antisense therapeutics to *in vitro* detection (2, 3).

The concept of therapeutic intervention at the level of nucleic acids has been advanced recently by spliceosome-mediated RNA trans-splicing (SMaRT) (4, 5). SMaRT has effectively repaired disease-causing mutant genes at the level of RNA splicing for several disorders including hemophilia and cystic fibrosis (6, 7). The principle behind SMaRT is centered on the use of engineered pre-trans-splicing molecules (PTMs), which can replace the mutated portion of a disease-causing gene with the wild-type sequence. SMaRT can also be used to regulate the trans-splicing and expression of almost any desired gene sequence, such as those encoding reporter or toxic molecules (4, 8). Embedded within each PTM are active splicing elements that are recognized by the cell's splicing machinery. These promote the formation of spliceosome complexes that trans-splice the PTM encoded exon(s) into the target transcript rather than allowing cis-splicing within the target pre-mRNA to occur. The specificity of the trans-splicing reaction is conferred primarily by the binding domain of the PTM, which is designed to be complementary to intronic sequences in the target of interest (8).

Building on the previous successes with therapeutic applications of SMaRT (6, 7), we decided to apply this platform technology to the field of molecular imaging by reprogramming expressed pre-mRNAs to encode reporter molecules that are used for imaging purposes. The rapidly emerging field of molecular imaging has concerned itself with designing strategies for noninvasively investigating molecular events on a global scale in living animals (9). To do so, various modalities are used, including cooled charge-coupled device (CCD) cameras for optical imaging, single-photon emission computed tomography (SPECT), and positron emission tomography (PET) for radionuclide imaging and MRI (9). Given the rapid production and highly modular nature of designing antisense oligonucleotide probes for nucleic acid targets, a key goal for this field is to develop a system for imaging any arbitrary nucleic acid sequence *in vivo*. Accomplishing this objective would allow investigators to target and image the expression of any gene of interest.

Our strategy for imaging mRNA with SMaRT technology has several advantages over more classical methods, such as radiolabeled antisense oligonucleotides (RASONs), but retains the specificity for targeting endogenous nucleic acids. Fig. 1 highlights the attributes of SMaRT for imaging endogenous mRNA. As a genetically encoded imaging system, SMaRT possesses the advantage of signal amplification at multiple steps (an attribute that antisense oligonucleotides do not have). Multiple hybrid proteins are translated for each composite mRNA produced, and if the protein encoded is an enzyme, each of these can convert many substrate molecules, resulting in multiple signals generated for each recognition event.

To demonstrate the potential of SMaRT for imaging the expression of an mRNA, we constructed a target gene consisting of a portion encoding for the *Renilla* luciferase bioluminescent protein coupled to intronic and exonic sequences from the human papillomavirus type 16 (HPV-16). *Renilla* luciferase was chosen because it has proven to be a very sensitive bioluminescent reporter (10). Sequences from HPV-16 were used because of their clinical relevancy and sequence familiarity. Expressed alone, the *Renilla* protein fragment does not possess any bioluminescent activity. To generate luciferase, we engineered a PTM containing the remaining portion of *Renilla* luciferase as a "3′ exon" and a binding domain specific for HPV-16. When the PTM trans-splices specifically into the target pre-mRNA, full-length *Renilla* luciferase mRNA and functional protein are produced, generating a bioluminescent signal. In this report, we show that SMaRT technology can create enzymatic activity and that the resultant signal can be detected both in cell culture and living animals.

Methods

Recombinant Pre-mRNA Target and Trans-Splicing PTM Constructs. To investigate the potential use of SMaRT for molecular imaging of gene expression, a model system was designed by using the synthetic *Renilla* luciferase (hRLuc) bioluminescent reporter

Abbreviations: SMaRT, spliceosome-mediated RNA trans-splicing; PTM, pre-trans-splicing molecules; RASON, radiolabeled antisense oligonucleotide; HPV, human papillomavirus; N2a, neuro-2a; ROI, region of interest; sr, steridian.

‡To whom correspondence should be addressed. E-mail: sgambhir@stanford.edu.

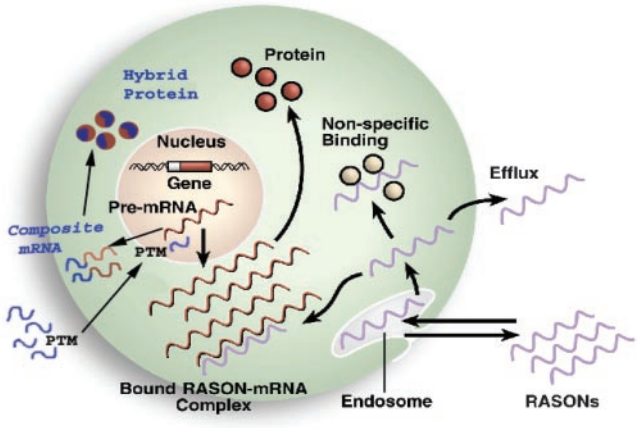

Fig. 1. Advantages of SMaRT over RASONs. RASONs are designed to hybridize to target mRNA to produce imaging signal. The SMaRT strategy uses trans-splicing of target mRNA to lead to hybrid proteins that are capable of being imaged. RASONs are limited in their use for *in vivo* imaging by several problems including nonspecific binding to proteins, a lack of efflux when no target mRNA encountered, and a limited amount of signal produced for each detection event. SMaRT has the advantages in delivery of a genetically encoded system as well as several stages of signal amplification that make it a more promising approach to *in vivo* imaging of mRNA.

gene. This prototype system is predicated on data that show that the hRLuc gene can be split into separate halves, which, if expressed individually, retain little to no bioluminescent activity in the presence of coelenterazine substrate (11). Thus, two plasmid constructs were generated, one that codes for the target pre-mRNA and contains the N terminus portion of the hRLuc gene as well as intronic and exonic sequences from the E6 and E7 oncoproteins of the HPV-16 (Fig. 2*A*). The other construct codes for the HPV target-specific PTM and contains the C terminus portion of the hRLuc gene as well as the components necessary to produce trans-splicing (Fig. 2*B*). These trans-splicing elements include a binding domain (BD) complementary to the target, a short spacer, and 3′ splice elements (branch point, polypyrimidine tract, and acceptor AG). The BD localizes the PTM and its active splice site to the vicinity of the target pre-mRNA. This interaction facilitates the specific trans-splicing reaction between splice sites in the target and PTM, splicing the C terminus portion of hRLuc adjacent to the N terminus portion, thus creating full-length *Renilla* luciferase (Fig. 2*C*).

The structures of LucHPVT3 and LucPTM37, as well as the proposed trans-splicing scheme between the two, are illustrated in Fig. 2. Both the target-expressing plasmid, pcLucHPVT3, and PTM-expressing plasmid, pcLucPTM37, were produced by ligating PCR-amplified fragments into the pcDNA3.1(−) vector backbone (Invitrogen). For the target plasmid, an 886-bp DNA fragment containing the N terminus portion of the humanized *Renilla* luciferase (hRLuc) was PCR-amplified from the phRL-SV40 vector (Promega). The primers used to produce the N terminus hRLuc insert were synthesized as follows: (Luc-16F) 5′-C TAG **GCT AGC** ATG GCT TCC AAG GTG TAC GAC CCC G, a 35-mer upstream primer introducing an *Nhe*I site (in bold) and with the underlined region homologous to nucleotides 1–24 of the hRLuc gene; (Luc-37R) 5′-C TAG **GGA TCC** *ACT TAC* CAC GAA GCT CTT GAT GTA CTT ACC CAT TTC, a 46-mer downstream primer introducing a *Bam*HI site (in bold) with the underlined region complementary to nucleotides 856–886 of the hRLuc gene and the italicized region coding for a 5′ donor site. Likewise, a 655-bp DNA fragment corresponding to portions of the E6 and E7 oncoproteins from human papillomavirus (HPV) type 16 was generated by using primers: (Luc-19F) 5′-C TAG **GGA TCC** GAC TTT GCT TTT CGG GAT TTA TGC, a 34-mer upstream primer introducing a *Bam*HI site (in bold) with the underlined region homologous to nucleotides 233–246 of the HPV gene target; (Luc-20R) 5′-C TAG **AAG CTT** TTA CTG CAG GAT CAG CCA TGG TAG, a 34-mer downstream primer introducing a *Hin*dIII site (in bold) with the underlined region containing a stop codon and complementary to nucleotides 866–880 of the HPV gene target. After amplification, the hRLuc PCR product was digested with *Nhe*I and *Bam*HI. Similarly, the HPV PCR product was digested with *Bam*HI and *Hin*dIII, and the pcDNA3.1(−) vector was digested with *Nhe*I and *Hin*dIII. The products of all three digestions were gel purified and then ligated to generate pcLucHPVT3.

To construct the PTM-expression plasmid, a 50-bp DNA fragment containing the C terminus portion of the hRLuc gene was PCR-amplified by using the following primers: (Luc-22F) 5′-C TAG **GAT ATC** *CAG* GTA AGT ACA TCA AGA GCT TCG, a 34-mer upstream primer introducing an *Eco*RV site (in

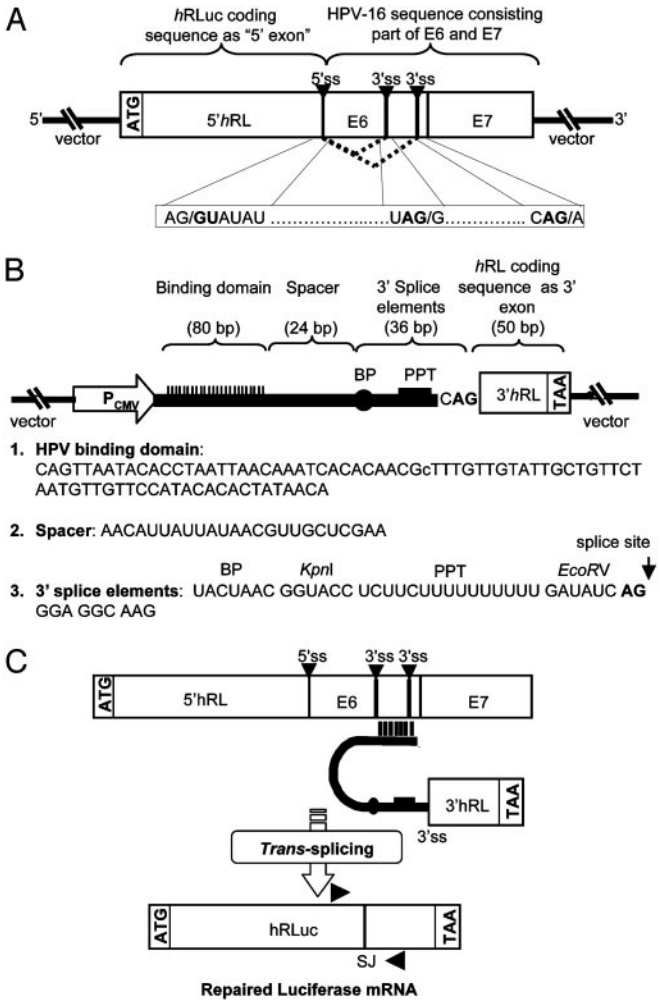

Fig. 2. Schematic diagrams of the PTM and pre-mRNA target used for imaging gene expression. (*A*) The pre-mRNA target, LucHPVT3, contains the N-terminal portion of hRLuc coding sequence coupled to exonic and intronic sequences of the HPV-16 E6 and E7 oncoproteins. Dotted lines indicate cis-splicing of the target. (*B*) LucPTM37 codes for the trans-splicing components (binding domain, spacer, and 3′ splice elements) as well as the C terminus portion of the hRLuc coding sequence. (*C*) Schematic representation of SMaRT reaction. Arrows indicate target (forward) and PTM (reverse) primers used for measuring specific trans-splicing. BP, branchpoint; PPT, polypyrimidine tract; ss, splice site; SJ, splice junction.

bold) with the underlined region homologous to nucleotides 887–907 and the italicized region introducing a 3′ splice acceptor site; (Luc-23R) 5′-C TAG **AAG CTT** TTA CTG CTC GTT CTT CAG CAC, a 31-mer downstream primer introducing a *Hin*dIII site (in bold) with the underlined region complementary to nucleotides 916–936 of hRLuc. To assemble the elements necessary for trans-splicing to occur (i.e., binding domain, spacer, branchpoint, and polypyrimidine tract) without any extraneous nucleotides, oligonucleotides were synthesized with *Nhe*I and *Eco*RV restriction sites at the 5′ and 3′ ends, respectively. The synthetic oligos were annealed by heating to 95°C and then allowed to cool to room temperature. The annealed oligos and hRLuc fragment were then ligated into an *Nhe*I- and *Eco*RV-digested pcDNA3.1(−) vector to generate pcLucPTM37.

Cell Culture and Transfections. Neuro-2a (N2a) mouse neuroblastoma cells were maintained in DMEM, supplemented with 10% FCS and 1% penicillin-streptomycin. To assess the ability of LucPTM37 to trans-splice into LucHPVT3, N2a cells were plated in 12-well plates, 60-mm dishes, or 100-mm dishes. Twenty-four hours later, the cells were transiently transfected with either pcLucHPVT3 or pcLucPTM37, or cotransfected with both pcLucHPVT3 and pcLucPTM37 by using SuperFect Transfection Reagent (Qiagen, Valencia, CA). Cells transfected with pCMV-hRL (Promega) were used as the positive control and mock-transfected cells were used as the negative control.

Luminometer Measurements. All bioluminescence assays were performed by using a TD 20/20 luminometer (Turner Designs, Sunnyvale, CA). Cells transfected in 12-well plates were lysed by using passive lysis buffer (Promega). Five microliters of cell lysate were mixed with 100 μl of coelenterazine (1 μg/ml in sodium phosphate buffer), and the reaction was measured in relative light units (RLU) over 10 s in the luminometer. Protein content of the cell lysate was measured by using Bio-Rad protein assay reagent (Bio-Rad Laboratories, Hercules, CA) in a Beckman DU-50 spectrophotometer (Beckman Coulter, Fullerton, CA), and luminescence results were reported as RLU per μg of protein per second.

Detection of Trans-Spliced Products by RT-PCR. To confirm that the intact hRLuc message was produced by trans-splicing, total RNA was isolated from cells transfected in 60-mm dishes or excised organs by using the RNeasy kit (Qiagen). RT-PCR was performed by using the EZ r*Tth* RNA PCR kit (Applied Biosystems) using 200 ng of total RNA and 100 ng each of the following primers designed to span the splice junction of the repaired hRLuc gene: (Luc-42F) 5′-GGA TAT CGC CCT GAT CAA GAG; or (Luc-41R) 5′-CTG CTC GTT CTT CAG CAC GCG. RT-PCRs were performed by using a PTC-200 Thermal Cycler (MJ Research, Reno, NV) and the following protocol: 60°C for 45 min, 94°C for 1 min, 35 cycles of 94°C (1 min), 48°C (1 min), 72°C (1 min), and a final extension step at 72°C for 15 min. The products were analyzed by gel electrophoresis using 2% agarose gels and stained with ethidium bromide. To confirm their identity, PCR bands were excised from the gels and sequenced by the UCLA Sequencing and Genotyping Core (University of California, Los Angeles).

Introduction of Transiently Transfected Cells Into Mice. All animal handling was performed in accordance with the University of California Los Angeles Animal Research Committee guidelines. Twenty-four hours after transfection, cells were collected by trypsinization, washed with PBS, counted, and then resuspended in PBS. Nude mice, ≈24 g in weight and 4 weeks old (Charles River Breeding Laboratories) were anesthetized by i.p. injections of ≈10 μl of a ketamine/xylazine (4:1) solution. After anesthetization, cells transiently transfected with pcLucHPVT3 (5×10^6 cells, suspended in 100 μl of PBS) or mock-transfected cells were implanted s.c. on the left and right side, respectively, of each animal's back ($n = 6$). Alternatively, mice were injected via the tail vein with cells (1×10^6 cells, suspended in 100 μl of PBS) transiently transfected with pcLucHPTV3 ($n = 8$) or mock-transfected cells ($n = 3$).

***In Vivo* Tf-PEI/DNA Polyplex Delivery of LucPTM37 to Mice.** The use of PEI polycation components for gene delivery has been described (12). Briefly, PEI components consisting of Tf-PEI25 and PEI22 (graciously provided by E. Wagner, Boehringer Ingelheim) were mixed in HBS buffer (75 mM NaCl/20 mM Hepes, pH 7.3) with 50 μg of pcLucPTM37 and incubated at room temperature for 20 min. Before injection, the complexes were adjusted with a 2.5% glucose solution to ensure physiologic iso-osmolarity. For the animals in which target-expressing cells were s.c. implanted, Tf-PEI-PTM37 complexes were injected via tail vein 24 h after target cell implantation and then scanned 24 h after Tf-PEI-PTM37 injection. For the animals in which target-expressing cells were injected intravenously, a subset ($n = 3$) was injected via tail vein with a single dose (1 dose = 50 μg pcLucPTM37) of the Tf-PEI-PTM37 complexes 4 h after cell injection. A second subset ($n = 3$) was injected with two doses, the first occurring 4 h after cell injection, and the second occurring 24 h after administration of the first dose. Both subsets of mice were scanned at 24, 48, and 72 h after the initial PTM injection. One subset ($n = 2$) of mice injected intravenously with target-expressing cells were scanned without being administered the Tf-PEI-PTM37 complexes to determine background levels of luminescence.

Imaging and Quantification of Bioluminescence. For small animal bioluminescence imaging, a Xenogen *in vivo* Imaging System (IVIS) (Xenogen, Alameda, CA) was used. Immediately before scanning, animals were anesthetized as before, and then injected via tail vein with coelenterazine (2.1 mg/kg of body weight). Animals were then placed directly in the imaging chamber, and whole body images were acquired for 5 min. Regions of interest (ROI) of constant area were manually drawn over areas of signal intensity by using the LIVING IMAGE software (Xenogen) and results were reported as maximum intensity values within an ROI in photons per second per cm^2 per steridian (sr).

Results

Reporter Gene Activity Is Restored by Trans-Splicing in Cell Culture. To evaluate the efficiency of the trans-splicing reaction, cells were transiently transfected with a plasmid expressing the pre-mRNA target, pcLucHPVT3, a plasmid expressing the PTM, pcLucPTM37, or both at a 1:1 ratio. Cells transfected with only the target or PTM plasmid showed minimal bioluminescence over background levels, indicating that cis-splicing of the target pre-mRNA does not result in functional *Renilla* luciferase and that the portion of hRLuc contained in the PTM is not sufficient for bioluminescent activity. When cells were cotransfected with both the target and PTM, a substantial gain in signal was observed. This strongly suggests that LucPTM37 is able to trans-splice into the LucHPVT3 pre-mRNA and reconstitute fully active *Renilla* luciferase. The luciferase signal produced by trans-splicing was compared against the signal from cells transfected with a plasmid coding for constitutively expressed full length hRLuc (pCMV-hRL) to estimate the efficiency of trans-splicing. Analysis revealed that the signal obtained from trans-splicing in cells co-transfected with both LucHPVT3 (target) and LucPTM37 (PTM) is ≈22–29% of the signal obtained from cells constitutively expressing full length hRLuc (Fig. 3A). As both the target pre-mRNA and PTM are under control of the CMV promoter, the pCMV-hRL control allows us to reasonably approximate trans-splicing efficiency. However, it is important

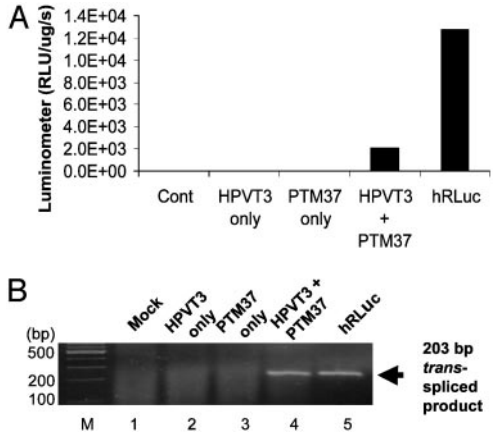

Fig. 3. mRNA repair and restoration of Luciferase function in cells. (*A*) Luminometer results reflecting the bioluminescence produced from hRLuc, generated by either the SMaRT trans-splicing reaction between HPVT3 and PTM37 or constitutively expressed full-length hRLuc. (*B*) RT-PCR results of fragments amplified by primers specific for opposite sides of the junction created by trans-splicing (lane 4). No evidence of trans-splicing was detected in mock-transfected cells or in cells transfected with plasmids expressing either target or PTM only (lanes 1–3).

to note here that this is not a measurement of trans-splicing efficiency alone. Rather, this estimation is a function, not only of trans-splicing efficiency, but also includes the transfection and transcriptional efficiency of the two plasmid system.

Little to no luciferase signal above background levels was detected in cells cotransfected with LucHPVT3 and a splice incompetent PTM that lacks functional 3′ splice elements (data not shown). These results further confirm that the luciferase signal observed in cotransfected cells is caused by trans-splicing between target pre-mRNA and PTM and is not caused by complementation of luciferase peptides separately expressed by the target and PTM.

RT-PCR Confirms Trans-Splicing Between Target Pre-mRNA and PTM in Cells. RT-PCR was performed to demonstrate that PTM-mediated trans-splicing generated full-length hRLuc transcripts. Twenty-four hours after transfection, total RNA was isolated from the cells, and hRLuc transcripts were amplified by RT-PCR with primers specific to opposite sides of the splice junction. Thus, only the products of trans-splicing reactions were amplified. Performing RT-PCR with primers Luc-42F/Luc-41R by using RNA isolated from cells expressing LucHPVT3 and LucPTM37 produced a product of 203 bp, which matched with the predicted product size generated with the same primers using RNA from cells transfected with pCMV-hRL (Fig. 3*B*, lanes 4 and 5). No specific product was detected in mock-transfected cells or in cells transfected with target or PTM only (Fig. 3*B*, lanes 1–3).

Trans-Splicing Can Be Imaged in Living Mice. Two experimental approaches were pursued to demonstrate that molecular imaging by trans-splicing could be achieved in living subjects. The first used s.c. implanted target-expressing cells as tumors in nude mice. A total of 5×10^6 N2a cells were transiently transfected with pcLucHPVT3 or mock transfected and then implanted bilaterally on the dorsal sides of mice ($n = 6$). Twenty-four hours after implantation, Tf-PEI-PTM37 polycation complexes were injected into the mice via the lateral tail-vein by using a poly(ethyleneimine) delivery system described elsewhere (12). Briefly, these polycation compounds complex with DNA because of their mutually attractive electric charges. By complexing

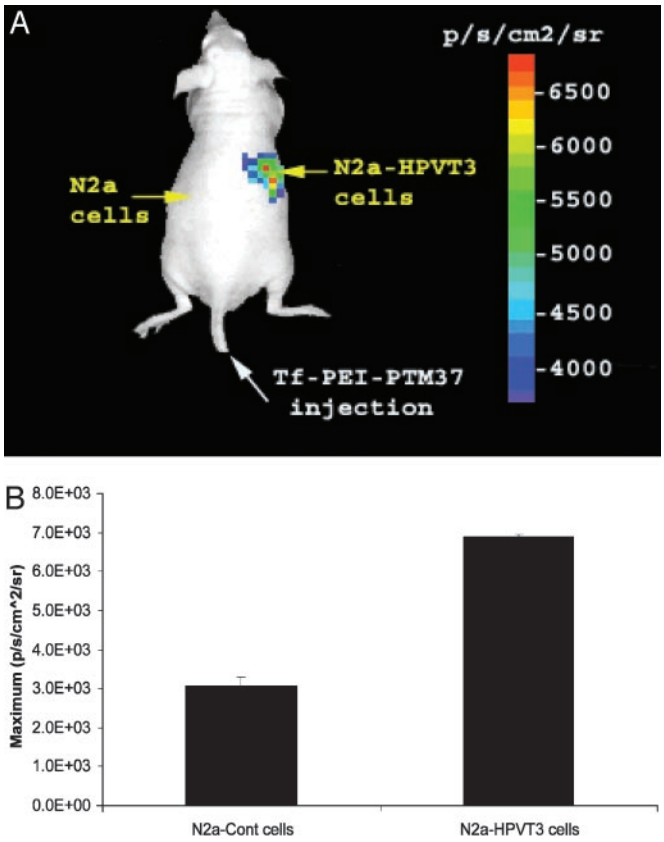

Fig. 4. Optical imaging of s.c. tumors in living mice using SMaRT. (*A*) Cells transfected with the pre-mRNA target LucHPVT3, or mock transfected were implanted s.c. onto different sides of a living mouse as shown. Twenty-four hours later, the mouse was injected with the Tf-PEI-PTM37 complexes via lateral tail vein, and then, 24 h after that, the mice were injected with coelenterazine and imaged by using a charge-coupled device camera. (*B*) ROI analysis of the maximum bioluminescent signal emitted from control and target-expressing tumors.

transferrin with the polycations, these compounds can selectively deliver DNA to cancer cells, which overexpress transferrin receptors. Twenty-four hours after PTM delivery, the mice were injected with coelenterazine and imaged by using a charge-coupled device (CCD) camera. As seen in Fig. 4*A*, the tumor site expressing the LucHPVT3 target emitted a detectable bioluminescent signal after LucPTM37 delivery. ROI analysis revealed that the signals from target-positive tumors are 2-fold greater than the background bioluminescence emitted from control tumors (Fig. 4*B*).

In the second approach, we examined whether trans-splicing could be observed in deeper tissues. To this end, we injected 1×10^6 N2a cells, transiently transfected with pcLucHPVT3, via the lateral tail vein into nude mice. Four hours after lateral tail-vein injection of the target-expressing cells, the Tf-PEI-PTM37 complexes were also injected via tail vein. Mice were then injected with coelenterazine substrate and scanned before PTM delivery and then again at 24, 48, and 72 h after LucPTM37 injection. Although it was predicted that the N2a-HPVT3 cells would become lodged in the lungs after i.v. administration, it was observed that bioluminescence was primarily emitted from the liver, before (Fig. 5*A*) and after (Fig. 5*B*) delivery of LucPTM37. This suggests that the N2a-HPVT3 cells travel throughout the vasculature until ultimately becoming lodged in hepatic tissue. Max-value ROI analysis revealed that the background bioluminescence produced by the N2a-HPVT3 cells in the liver is 1.1 ×

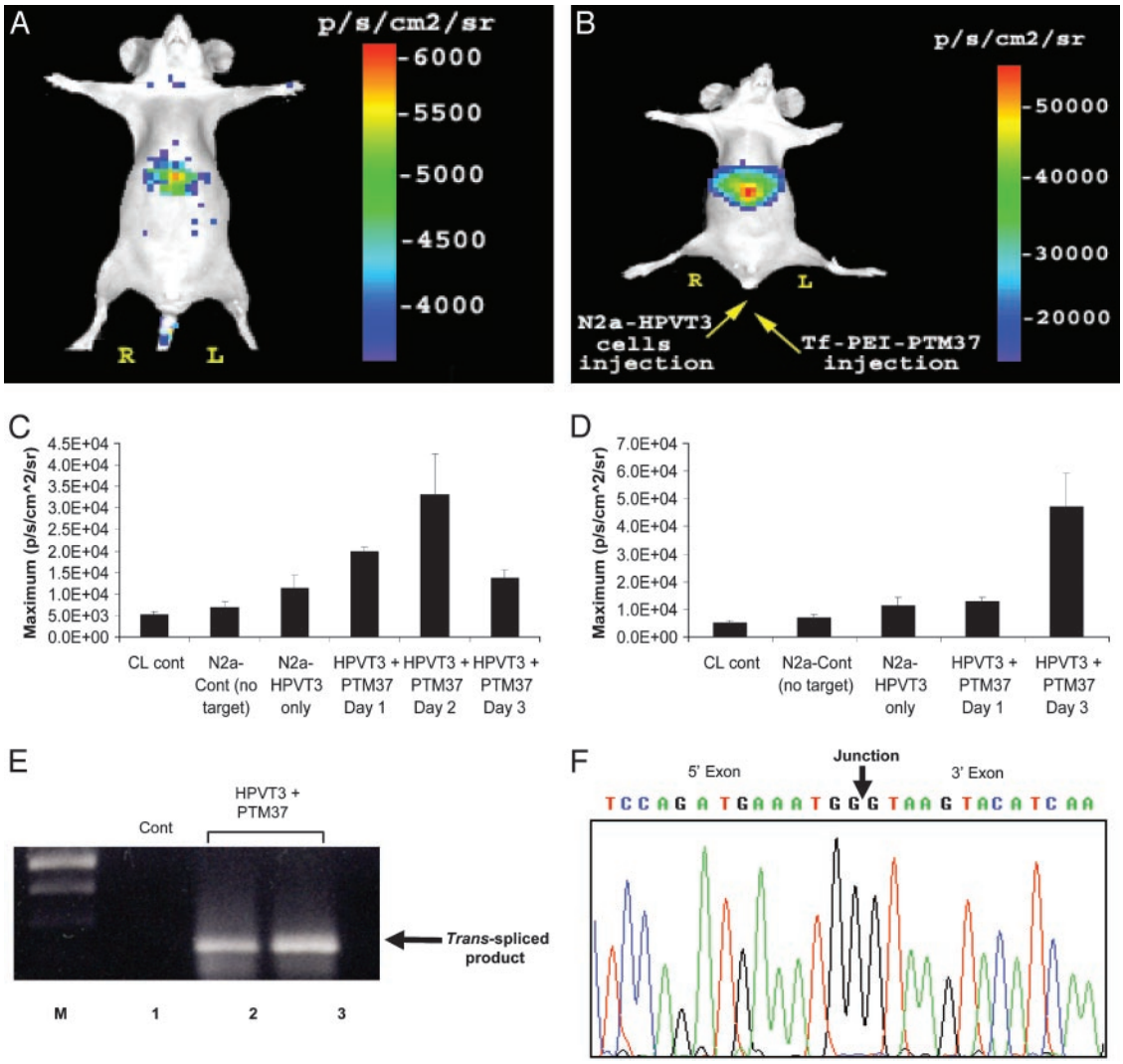

Fig. 5. Optical cell trafficking imaging using SMaRT. (*A*) Background bioluminescence produced by cells transiently transfected with LucHPVT3 and injected into a living mouse via the tail vein. (*B*) Bioluminescence observed in the same mouse seen in *A*, 48 h after injection of Tf-PEI-PTM37 complexes. (*C*) ROI analysis of bioluminescent signals emitted as a function of time after PTM-injection. The signal peaks at 2 days after injection and then subsides by day three. (*D*) Effects of multiple PTM-injections as assessed by ROI. Maximum signal is achieved by injecting a second PTM dose 24 h after the first PTM dose, and then imaging 48 h after the final injection. (*E*) RT-PCR results using total RNA isolated from the liver of mice injected with either zero (lane 1), one (lane 2), or two (lane 3) doses of Tf-PEI-PTM37 and using primers specific for opposite sides of the junction created by trans-splicing. (*F*) Sequencing results of RT-PCR products seen in *E*. Sequence analysis confirmed that the bands produced by RT-PCR are identical to the hRLuc sequence.

$10^4 \pm 3.0 \times 10^3$ p/s/cm^2/sr (Fig. 5*C*). After a single dose of LucPTM37, the maximum signal was observed at 48 h ($3.3 \times 10^4 \pm 9.3 \times 10^3$ p/s/cm^2/sr) and then subsided by 72 h after injection ($1.3 \times 10^4 \pm 1.7 \times 10^3$ p/s/cm^2/sr) (Fig. 5*C*). In an attempt to maximize the signal, we studied the effect of multiple doses of LucPTM37. A subset of mice injected intravenously with N2a-HPVT3 cells was given two doses of LucPTM37, with the first dose administered 4 h after target cell delivery, and the second dose given 24 h after the first (Fig. 5*D*). Max-value ROI analysis revealed that, within 48 h after the second LucPTM37 dose, the bioluminescent signal from the liver ($4.7 \times 10^4 \pm 1.7 \times 10^3$ p/s/cm^2/sr) was ≈1.4-fold greater than highest signal observed in the mice given only a single PTM dose (Fig. 5*D*).

RT-PCR Confirms Trans-Splicing in Living Mice. To confirm that the bioluminescent signals observed from the livers of the mice injected intravenously with N2a-HPVT3 cells were produced by trans-splicing, RT-PCR was performed on total liver RNA by using target- and PTM-specific primers as described above. RT-PCR analysis revealed the expected 203-bp product only in mice injected with LucPTM37 (Fig. 5*E*, lanes 2 and 3), but not from control mice injected only with target-expressing cells (Fig. 5*E*, lane 1). Direct sequencing of the product demonstrated the correct full-length hRLuc sequence, thereby confirming the accuracy of trans-splicing (Fig. 5*F*).

Discussion

SMaRT technology has been demonstrated to be a powerful and promising tool for gene therapy (13). Coupled with molecular imaging, it also has potential as a diagnostic platform to image gene expression (5). We have demonstrated in this report that the products of trans-splicing can be imaged in living animals, not only in s.c. tumors, but also in deeper tissues such as the liver. Although the model system provided here is not immediately applicable to universal imaging of any arbitrary mRNA target, our work presents an important step toward that goal.

Until now, attempts at imaging endogenous mRNA *in vivo* have met with limited success. A number of efforts have been

made to image endogenous genes with RASONs (14, 15). These molecules are generally modified nucleic acids (e.g., phosphorothioates, 2′-OMe backbone, peptide nucleic acids) that have been labeled with a radioisotope (e.g., F^{18}, In^{111}, Tc^{99m}). The principle behind imaging with RASONs is straightforward; a RASON can be designed to target an arbitrary sequence, then delivered systemically. The RASON will distribute throughout the organism and bind to the target sequence. Excess RASONs are eliminated from the organism, and the residual image reflects the location and level of expression of the gene of interest. The applicability of these molecules for imaging gene expression, however, is limited by their pharmacological properties. RASONs encounter several obstacles before reaching their targets, including degradation by nucleases and cellular impermeability. They also have nonspecific interactions and do not always efflux well from cells that do not contain the target mRNA.

The use of SMaRT technology and PTMs bypasses some of these hurdles because the targeting and reporter molecules are genetically encoded. Thus, SMaRT imaging can be reduced to a problem of gene delivery. To use gene delivery to accomplish global imaging of a particular gene's expression, care must be taken in choosing an appropriate vehicle for delivery as well as promoter for expression. If either the vehicle or the promoter chosen have distinct properties in various tissues, the results of such an image might obscure the true underlying biological processes. Using a constitutive promoter, known to drive expression robustly in many different tissues (as was done in this study with the CMV promoter), evades one of these problems. Although the science of transgene delivery has not yet been perfected, significant progress has been made over the last several years. Delivering the reporter molecule as a transgene greatly reduces the number of variables in the equation, thus making the goal of imaging mRNA more feasible. Signal amplification is another advantage of using SMaRT to image mRNA, because multiple signals are generated for each trans-splicing event. A RASON can at most produce as many signals as there are isotopes linked per RASON, and this is usually a single isotope. However, when a PTM splices into its target, the reporter gene encoded can be translated into multiple copies of an enzyme, which, in the presence of its substrate, can produce thousands of signals. This signal amplification, coupled with the modularity of SMaRT that facilitates the targeting of a wide variety of endogenous mRNA and potentially allows the use of many different reporter genes (e.g., multimodality fusion reporter genes; ref. 16), makes this method for imaging mRNA significantly more attractive than previously described approaches. In the current work, we did not normalize for transfection efficiency because the vectors used are in the same backbone and of comparable size. Under these conditions, we have found that transfection efficiency only accounts for 5–7% of the observed differences (unpublished data).

This study represents an important proof-of-concept in the overall scheme of developing SMaRT as a platform technology to image endogenous genes. Although we did not image an endogenous mRNA, this work demonstrates that trans-splicing can be used to image gene expression in living subjects. The success of this work was aided by targeting an exogenous gene, driven by a strong, constitutive promoter, and further experiments will strive to image endogenous genes that may not have such high levels of expression. Future studies will have to explore sensitivity of this assay as a function of number of target mRNAs. To accomplish this task, we must better understand the rules necessary to design and create PTMs that are specific to any target mRNA sequence of interest, and can deliver a full-length reporter that remains inactive until trans-splicing occurs. Toward this end, we are developing a functional genetic screen to rapidly screen millions of different sequence combinations to identify optimal PTMs with improved specificity and efficiency. This high-throughput screen coupled with rational design should permit the rapid development of a probe for any mRNA of interest, to report on the localization and magnitude of its expression. The applications for such a tool could advance a number of imaging-related areas of investigation, such as cell traffic monitoring, *in vivo* drug screening, and more sensitive noninvasive real-time diagnostics. A more immediate use of this technology is imaging the event of trans-splicing itself. Pairing a full-length reporter gene with PTMs designed for therapeutic uses would give investigators the ability to correlate the degree of gene repair by SMaRT with the level of reporter gene expression. Thus, established methods of noninvasive imaging could be used to monitor the gene therapy provided by SMaRT with hardly any modification. Given its advantages over other methods for imaging mRNA *in vivo*, together with its applicability to other active areas of investigation, SMaRT has the potential for becoming an essential implement in the molecular imaging toolbox.

This work was supported by National Institutes of Health Grant R01CA82214-05 and Department of Energy Grant DE-FG02-03ER63687 (to S.S.G.).

1. Southern, E. M. (1975) *J. Mol. Biol.* **98,** 503–517.
2. Stephens, A. C. & Rivers, R. P. (2003) *Curr. Opin. Mol. Ther.* **5,** 118–122.
3. Joos, L., Eryuksel, E. & Brutsche, M. H. (2003) *Swiss Med. Wkly.* **133,** 31–38.
4. Puttaraju, M., Jamison, S. F., Mansfield, S. G., Garcia-Blanco, M. A. & Mitchell, L. G. (1999) *Nat. Biotechnol.* **17,** 246–252.
5. Otto, E., Temple, G. F. & McGarrity, G. J. (2003) *Current Drug Discovery*, 37–42.
6. Chao, H., Mansfield, S. G., Bartel, R. C., Hiriyanna, S., Mitchell, L. G., Garcia-Blanco, M. A. & Walsh, C. E. (2003) *Nat. Med.* **9,** 1015–1019.
7. Liu, X., Jiang, Q., Mansfield, S. G., Puttaraju, M., Zhang, Y., Zhou, W., Cohn, J. A., Garcia-Blanco, M. A., Mitchell, L. G. & Engelhardt, J. F. (2002) *Nat. Biotechnol.* **20,** 47–52.
8. Puttaraju, M., DiPasquale, J., Baker, C. C., Mitchell, L. G. & Garcia-Blanco, M. A. (2001) *Mol. Ther.* **4,** 105–114.
9. Massoud, T. F. & Gambhir, S. S. (2003) *Genes Dev.* **17,** 545–580.
10. Bhaumik, S. & Gambhir, S. S. (2002) *Proc. Natl. Acad. Sci. USA* **99,** 377–382.
11. Paulmurugan, R. & Gambhir, S. S. (2003) *Anal. Chem.* **75,** 1584–1589.
12. Hildebrandt, I. J., Iyer, M., Wagner, E. & Gambhir, S. S. (2003) *Gene Ther.* **10,** 758–764.
13. Garcia-Blanco, M. A. (2003) *J. Clin. Invest.* **112,** 474–480.
14. Touboul, M., Gauchez, A. S., D'Hardemare Adu, M., Lunardi, J., Deverre, J. R., Pernin, C., Mathieu, J. P., Vuillez, J. P. & Fagret, D. (2002) *Anticancer Res.* **22,** 3349–3356.
15. Dewanjee, M. K., Haider, N. & Narula, J. (1999) *J. Nucl. Cardiol.* **6,** 345–356.
16. Ray, P., Wu, A. M. & Gambhir, S. S. (2003) *Cancer Res.* **63,** 1160–1165.